Science & Technology Development Journal 2025, 28(3):3779-3785

Open Access Full Text Article

Research Article

Research and synthesis of popcorn-like Ag@CZZ nanomaterial for detecting tebuconazole

Bao Tran Nguyen[1,2,3], Nguyen Do Quynh Nhu [1,2,3], Thao Anh Do[2,3], Hong Tho Le[2,3], Hanh Kieu Thi Ta[1,2,3], Quang Ngoc Tran[2,3], Nhu Hoa Thi Tran[1,2,*]

ABSTRACT

Introduction: Pesticide residues in food remain a persistent, unresolved concern related to public health. Porous materials such as metal-organic frameworks (MOFs), combined with the localized surface plasmon resonance (LSPR) effect of silver nanoparticles (Ag NPs), enable label-free detection of analyte concentrations with high sensitivity. This approach is particularly effective for detecting tebuconazole (TB) residues, a persistent fungicide that poses significant environmental and food safety risks.

Methods: Ag NPs were synthesized in a pre-prepared zeolitic imidazolate framework (ZIF) solution using a chemical reduction method, achieving relatively high uniformity. For surface-enhanced Raman scattering (SERS) applications, a self-assembled monolayer coating was fabricated on filter paper (FP) substrates by leveraging the strong absorption of Ag@Co-Zn-ZIF (Ag@CZZ) nanocomposites on cellulose fibers.

Results: UV–vis spectroscopy revealed that the LSPR wavelength of the Ag NPs is 419 nm, while XRD analysis confirmed the (111) plane of the face-centered cubic (FCC) crystalline structure of Ag. Morphologically, the synthesized NPs exhibited a unique ``popcorn-like'' structure with an average size of approximately 408 nm, determined by field-emission scanning electron microscopy (FE-SEM). Energy-dispersive X-ray spectroscopy (EDS) showed the presence of elements constituting the popcorn-like Ag@CZZ. Moreover, characteristic vibrations from the ZIF structure were identified in the Raman spectra. The FP/Ag@CZZ SERS substrate for monitoring TB concentration was successfully established, with a calculated limit of detection (LOD) of 3.08×10^{-8} M.

Conclusion: Leveraging the LSPR effect of Ag NPs and the structural properties of ZIF, a simple and rapid fabrication method was employed to develop a flexible and effective FP/Ag@CZZ SERS substrate. This platform exhibited high sensitivity in detecting and monitoring changes in TB concentration, indicating promising potential for improving the detection limits of pesticide residues in agricultural and environmental monitoring.

Key words: Co-Zn-ZIF, Ag@CZZ, Popcorn-like, Tebuconazole

[1]*Faculty of Materials Science and Technology, University of Science, Ho Chi Minh City, Vietnam*

[2]*Vietnam National University, Ho Chi Minh City, Vietnam*

[3]*Center for Innovative Materials and Architectures (INOMAR), Ho Chi Minh City, Vietnam*

Correspondence

Nhu Hoa Thi Tran, Faculty of Materials Science and Technology, University of Science, Ho Chi Minh City, Vietnam

Vietnam National University, Ho Chi Minh City, Vietnam

Email: ttnhoa@hcmus.edu.vn

History

- Received: 12-05-2025
- Revised: 25-06-2025
- Accepted: 05-07-2025
- Published Online: 20-08-2025

DOI :

https://doi.org/10.32508/stdj.v28i3.4485

INTRODUCTION

Tebuconazole (TB) is a widely used triazole fungicide that has attracted attention due to its persistence in soil and water, as well as its potential for bioaccumulation[1]. Excessive or improper use of TB has been shown to lead to environmental contamination, posing risks to ecosystems by disrupting microbial communities and affecting non-target organisms[2]. Moreover, exposure in humans, particularly at levels exceeding regulatory limits, has been associated with adverse health effects, including endocrine disruption[3] and potential carcinogenicity[4]. These concerns underscore the urgent need for reliable and sensitive detection methods that can detect TB residues at very low concentrations.

Metal-organic frameworks (MOFs) have gained significant attention over the past decade as a unique class of crystalline materials composed of metal ions or clusters coordinated with organic linkers. Their high porosity, large surface area, and structural tunability make them extraordinarily versatile for a range of applications, including gas storage, catalysis, and separation[5]. Moreover, the diversity of organic linkers enables the incorporation of multifunctional sites for specific chemical interactions, offering significant potential for sensing applications. Researchers have increasingly focused on leveraging the properties of MOFs to develop advanced composites that can detect trace levels of target analytes in various matrices, including complex environmental and biological samples[6].

The combination of MOFs with silver (Ag) has emerged as a promising strategy to achieve enhanced detection capabilities. Ag nanostructures exhibit

Cite this article : Nguyen B T, N D Q N, Do T A, Le H T, Ta H K T, Tran Q N, Tran N H T. **Research and synthesis of popcorn-like Ag@CZZ nanomaterial for detecting tebuconazole**. *Sci. Tech. Dev. J.* 2025; 28(3):3779-3785.

strong localized surface plasmon resonance (LSPR), which substantially amplifies electromagnetic fields near their surfaces[7]. When integrated into MOF frameworks, these Ag nanoparticles (NPs) can be more uniformly dispersed and stabilized, thereby preventing agglomeration and maintaining high surface-enhanced Raman scattering (SERS) activity over prolonged periods[8]. The hierarchical porosity of MOFs facilitates the efficient mass transfer of analytes to the Ag active sites, while the MOF matrix also provides selective binding sites for specific molecules[9]. Consequently, Ag-MOF composites offer an optimal architecture that combines the intrinsic high porosity of MOFs with the enhanced plasmonic properties of Ag. Surface-enhanced Raman scattering (SERS) has proven to be an indispensable technique for the detection of low concentrations of various compounds in fields such as food safety[10], environmental monitoring[11], clinical diagnostics[12]. In SERS, the vibrational signatures of target molecules are substantially amplified when they are adsorbed onto nanostructured metal surfaces[13]. This powerful enhancement allows the detection of analytes at levels that are too low for conventional Raman spectroscopy. Employing Ag-MOF composites can further enhance both reproducibility and sensitivity, as the porous structure of the MOF ensures a uniform distribution of hotspots, resulting in more consistent signal intensities across measurement sites.

By leveraging the combined benefits of MOFs and Ag, SERS-based sensors can potentially provide a rapid, selective, and highly sensitive method for detecting TB in complex matrices. The porous MOF scaffold ensures that analytically relevant amounts of TB come into contact with the plasmonic assets of Ag, thus producing enhanced Raman signals. This innovative approach addresses current challenges in pesticide detection and may also be suitable for broader applications in monitoring other environmental and food contaminants. In this study, we explore the design and fabrication of an Ag-MOF composite tailored for SERS detection and demonstrate its effectiveness in detecting TB, highlighting its potential as a powerful tool for ensuring environmental safety and public health.

EXPERIMENTAL

Chemical and reagent

The chemicals and materials used in this study include silver nitrate ($AgNO_3$, 99.9%), zinc nitrate hexahydrate ($Zn(NO_3)_2.6H_2O$, 98%), 2-methylimidazole ($C_4H_6N_2$, 99%), cobalt nitrate hexahydrate ($Co(NO_3)_2{\cdot}6H_2O$, 98%), polyvinylpyrrolidone ($(C_6H_9NO)_n$, 99%), and ascorbic acid ($C_6H_8O_6$, 99%), all of which were purchased from Sigma-Aldrich Co., MO, USA. Ethanol (C_2H_5OH, 99.8%) and methanol (CH_3OH, 99%) were supplied by Fisher Ltd. (UK). The filter paper employed in this study was supplied by Hangzhou Special Paper Industry Co., Ltd. (Grade 102). It was characterized by a medium texture, a maximum pore size ranging from 15 to 20 μm, a filtration speed of 25 to 70 seconds, an ash content of $\leq$ 0.15%, and a basis of 80 $\pm$ 4 g/m^2.

Synthesis process of Ag@CZZ

The Co-Zn-ZIF (CZZ) solution was synthesized by mixing $Zn(NO_3)_2.6H_2O$ (0.47 g), $Co(NO_3)_2.6H_2O$ (0.29 g), $(C_6H_9NO)_n$ (1.03 g), and $C_4H_6N_2$ (0.57 g) in 100 mL of methanol. In the solution, $C_4H_6N_2$ was used as a material particle size controller. After continuously stirring for 24 hours, the CZZ sample was recovered by centrifugation and washed five times in methanol. After centrifugation and vacuum drying at 80 °C overnight, the obtained solid product weighed 0.0332 g (as shown in Figure 1a), corresponding to a reaction mass efficiency (RME) of 21.18 % based on the total mass of zinc salt, cobalt salt, and linker. The RME was employed to evaluate the process efficiency according to Eq.1[14].

$$RME = \frac{m_{CZZ}}{m_{Zn}+m_{Co}+m_{linker}} \times 100 \quad (1)$$

where m_{Co}, m_{Zn}, and m_{linker} are masses of synthetic material and precursor materials ($Zn(NO_3)_2.6H_2O$ (0.47 g), $Co(NO_3)_2.6H_2O$, and 2-methylimidazole linkers), respectively.

The popcorn-like Ag@Co-Zn-ZIF (Ag@CZZ) material was synthesized according to the following steps. First, the CZZ was dispersed in 50 mL of methanol. After that, solution A consisted of 0.0213 g ascorbic acid dispersed in 12 mL of CZZ, while 0.01853 g of $AgNO_3$ was dissolved in 12 mL of CH_3OH and referred to as solution B. Second, solution B was dropped into solution A and subjected to ultrasonication for 15 minutes. Third, the Ag@CZZ was recovered by centrifugation and washed five times in methanol, as shown in Figure 1b.

SERS measurement

The sensor substrate was fabricated using a filter paper-based platform, as illustrated in Figure 2. The filter paper (FP) was cleaned with ethanol and dried before use. The FP was then immersed in the Ag@CZZ solution for 2 hours and dried at room temperature for 1 hour to form the FP/Ag@CZZ SERS substrate.

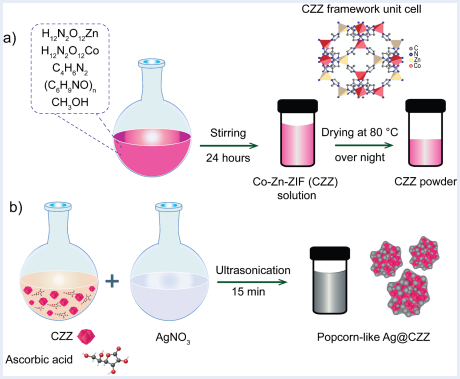

Figure 1: Schematic of the fabrication process: (a) Co-Zn-ZIF (CZZ), (b) popcorn-likeAg@CZZ material

For SERS measurements, 20 μL of TB solution at each concentration from 10^{-3} M to 10^{-7} M was dropped onto the surface of the FP/Ag@CZZ SERS substrate for each measurement, and the analyte was then dried at room temperature. The Raman spectra of the analytes were recorded using an inVia confocal Raman microscope manufactured by Renishaw (Wotton-under-Edge, UK) at a wavelength of 633 nm, a HeNe laser power of 5 mW, and a spectral acquisition time of 10 seconds. All experiments were conducted under identical conditions to ensure reproducibility. The analyte was evenly distributed on the flat SERS substrate and allowed to dry at room temperature for 1 hour. The experiment utilized 20 mL of analyte at varying concentrations. In this study, TB was analyzed using Raman spectroscopy within the concentration range of 10^{-3} M to 10^{-7} M. Measurements were randomly obtained at five different positions on the FP/Ag@CZZ substrate, corresponding to the analyte concentrations within the investigated range.

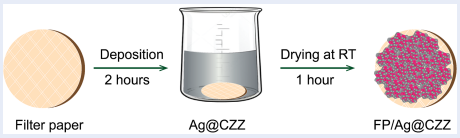

Figure 2: Fabrication process of FP/Ag@CZZ substrate

RESULTS

The optical characteristics in the UV-Vis spectrum (Figure 3a) showed that the synthesized CZZ exhibited a maximum absorption peak at 590 nm and a small satellite peak at 544 nm. In contrast, the Ag@CZZ sample revealed a broad absorption peak in the wavelength range of 400 nm to 425 nm; however, no absorption peak corresponding to CZZ was observed, which may be a result of the strong optical dominance of Ag in the Ag@CZZ material. The XRD pattern results (Figure 3b) were used to investigate the crystalline properties and purity of the products within the 2θ angle range from 5° to 50° for the CZZ, and Ag@CZZ samples, as shown inFigure 3b.

The surface morphology characteristics and elemental composition of Ag@CZZ were evaluated through field-emission scanning electron microscopy (FE-SEM) images. After synthesis, the FESEM images revealed the distribution of Ag@CZZ particles, exhibiting a popcorn-like morphology, as shown in Figure 4a. Additionally, the particle size distribution graph and the elemental mapping of samples are presented in Figure 4b-c, respectively.

Figure 5a displays the comparative Raman spectra of three distinct samples: Raman spectra of TB powder, Ag@CZZ popcorn-like, and SERS of TB (10^{-3} M) used as a reference. Notably, the Ag@CZZ substrate enables the detection of TB down to a concentration of 10^{-7} M, with characteristic peaks observed at 441 cm^{-1}, 1203 cm^{-1}, 1068 cm^{-1}, and 1622 cm^{-1}. Linear calibration plots corresponding to the three most intense peaks are illustrated in Figure 5b-c.

DISCUSSION

The UV-Vis spectra of CZZ material (Figure 3a) exhibit a maximum absorption band in the wavelength range of 520–600 nm due to the energy level transition of Co^{2+} [15]. After combining, the Ag@CZZ (Figure 3a) exhibits a broader absorption peak. The wavelength range of 400–460 nm corresponds to the energy transition of 4d and 5s electrons of Ag to higher energy levels [16,17]. Additionally, the characteristic absorption peak of CZZ at 590 nm disappears, indicating an interaction between Ag and CZZ; this interaction leads to molecular resonance, causing a blue shift in the spectrum. In Figure 3b, the CZZ exhibits characteristic diffraction peaks at 2θ angles of 7.38°, 10.48°, 12.76°, 14.75°, 16.49°, and 18.06° at the (110), (002), (112), (022), (013), and (222) crystal planes, respectively [15,18]. Meanwhile, the XRD pattern of Ag@CZZ only shows the diffraction peak at 38.2°, corresponding to the (111) crystal planes of the face-centered cubic (FCC) structure of Ag (JCPDS fileno. 04-0783) [19], and the diffraction peaks at 2θ = 12.5° ([101]) and 2θ = 22° ([002], [101]) corresponding to the structure of cellulose [20].

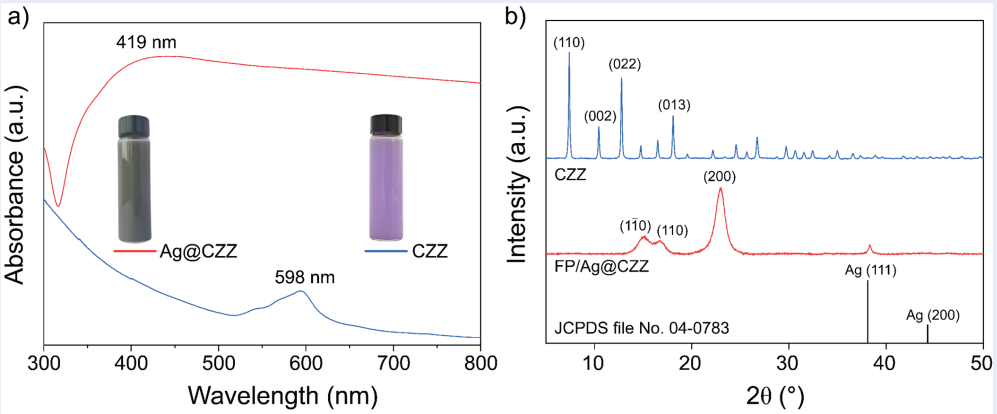

Figure 3: (a) UV-Vis spectrum, (b) XRD pattern of Ag@CZZ and CZZ samples

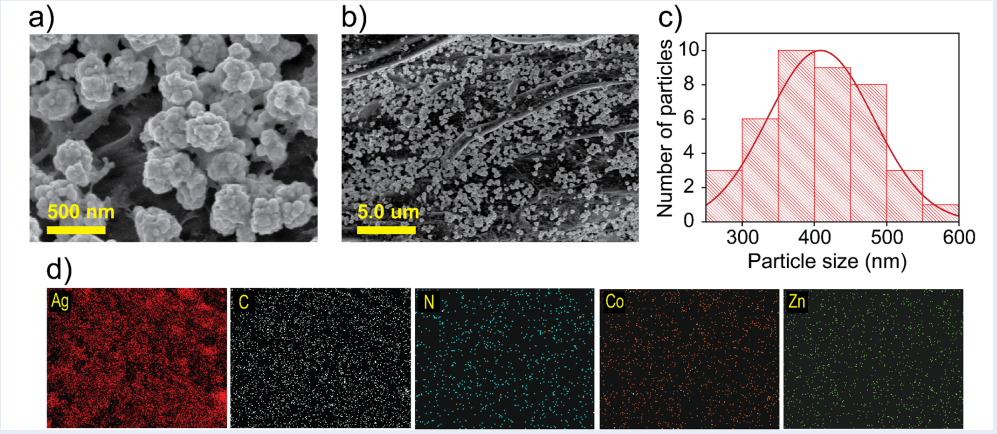

Figure 4: (a-b) FESEM images on filter paper substrate; (c) particle sizedistribution graph, and (d) EDS mapping of an Ag@CZZ sample

The surface morphology of Ag@CZZ shown in Figure 4a-b indicates that the material has a non-agglomerated "popcorn-like" shape that is physically adsorbed throughout the surface of the filter paper. The particle size distribution graph in Figure 4c shows that the average size of Ag@CZZ is approximately 408 nm. In Polavarapu et al.,[21] cellulose is employed as a robust supporting platform for immobilizing synthesized plasmonic NPs via various techniques, including thermal evaporation, vapor deposition, laser-induced photothermal deposition, dip-coating, inkjet printing, and screen printing. In recent studies, cellulose in various forms has also been employed as a stabilizing agent to prevent NP aggregation during plasmonic NP synthesis in the presence of reducing agents[21–24]. Researchers have also explored the design of cellulose-based SERS substrates to produce commercially viable, sustainable, flexible, and environmentally friendly platforms in the future. In this work, the use of FP as a platform for decorating with Ag@CZZ NPs is also essential in stabilizing these plasmonic NPs. The rough surface with grooves and gaps between cellulose fibers, along with the abundance of hydroxyl (-OH) groups across the FP surface, helps anchor the Ag@CZZ NPs, enabling widespread distribution across the substrate while reducing agglomeration, thus preserving the popcorn-like morphology as initially intended.

In Figure 5a, most of the observed vibrational peaks in the Raman spectrum originate from the vibrations of methyl groups and the imidazole ring. The Raman spectrum of the Ag@CZZ sample shows peaks at 282 cm^{-1} and 428 cm^{-1}, corresponding to the Zn–N and Co–N stretching mode, respectively[25,26].

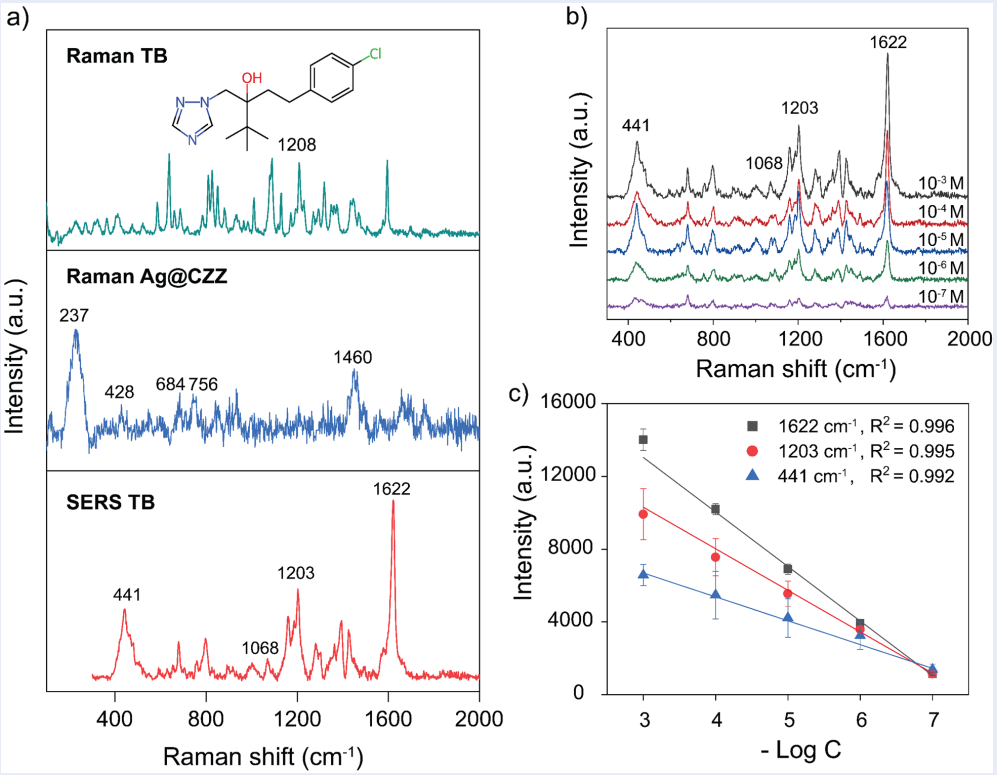

Figure 5: (a) Raman spectra of TBpowder and molecular structure (insert), Ag@CZZ substrate, and SERS spectrum ofTB at 10^{-3} M; (b) SERS spectra; (c) standard curve of TB at variousconcentrations.

In addition, the peaks observed at 685 cm^{-1}, 1146 cm^{-1}, and 1460 cm^{-1} correspond to imidazolium ring puckering, C–N stretching, and methyl bending of 2-methylimidazole ligand, respectively[27]. Although CZZ is not observed in the UV-Vis spectrum and XRD pattern, EDS mapping and Raman spectroscopy confirm its presence in the obtained product, indicating the successful incorporation of Ag composition into the ZIF framework. The SERS spectrum of TB at a concentration of 10^{-3} M (Figure 5a) indicates that the vibrational modes of TB have shifted to higher wavenumbers. This observation can be attributed to the Raman peak shift phenomenon, which may arise from alterations in the molecular structure. The interaction between TB and Ag@CZZ can generate by-products, demonstrated by the peaks at 1620 cm^{-1}, 1068 cm^{-1}, and 796 cm^{-1} which indicate the presence of oxidation products such as hydroxybenzoic acid derivatives originating from the oxidation of aliphatic carbons directly linked to the phenyl group[28]. In addition, changes in the electronic environment when TB interacts with Ag on the CZZ framework can also occur due to the binding ability of TB molecules through the triazole group. This leads to changes in the direction of molecular vibrations and the degree of electron cloud overlap at the Ag@CZZ surface. The nitrogen atom within the triazole ring could donate electrons to interact with the surface Ag atoms, thereby modifying the electron density and force constants, resulting in the observed peak shifts. For instance, the torsion mode of CN at 1262 cm^{-1} suggests an enhanced interaction involving the triazole region. Furthermore, the C–N, C–C, and CH_2 stretching vibrations shift from 1230 cm^{-1} to 1203 cm^{-1}, which is consistent with the proposed hypothesis[29].

To investigate the SERS detection sensitivity of the Ag@CZZ substrate, the SERS spectrum of TB is recorded at concentration range of 10^{-7} M to 10^{-3} M. Figure 5b shows that the Raman scattering signal intensity decreases with concentration, the characteristic peaks at 1622 cm^{-1}, 1202 cm^{-1}, and 441 cm^{-1} remain discernible even at a concentration as low as 10^{-7} M. The high Raman peaks at 1622, 1203, and 441 cm^{-1} were selected to evaluate the calibration characteristics. The calibration graphs in Figure 5c show a statistical linear dependence of the three Raman peak

intensities on TB concentration, with correlation values (R^2) all greater than 0.99. The LOD is calculated to be 3.08×10^{-8} M.

The LOD of tebuconazole detection achieved in this study (3.08×10^{-8} M) is relatively higher than some previously reported values using commercial substrates or another techniques (Table 1), our work introduces a novel popcorn-like Ag@CZZ nanostructure synthesized via a simple, cost-effective method and flexibility of the filter paper-based SERS substrate also demonstrates its potential for practical applications, such as conducting tests on rough surfaces. This novel provides enhanced hot-spot density and uniform particle distribution, which can be further optimized to improve detection performance. These results demonstrate that the SERS platform based on FP/Ag@CZZ exhibits excellent sensitivity for the detection of TB.

Table 1: LOD comparison between TB detection sensors

Method	LOD (M)	References
Aptasensor	1.0×10^{-8}	30
Lateral flow immunoassay	2.44×10^{-7}	31
LC–MS/MS	4.88×10^{-9}	32
Voltammetric	1.5×10^{-7}	33
Biosensor	1.62×10^{-8}	34
SERS	3.25×10^{-9}	35
	2.92×10^{-7}	36
	1.4×10^{-6}	37
	1.43×10^{-8}	38
	3.08×10^{-8}	This work

CONCLUSIONS

In this study, we successfully developed a Ag@CZZ material and a flexible FP/Ag@CZZ SERS substrate. A novel and prominent feature of this sensor is its extremely simple and time-efficient fabrication process, along with its unique "popcorn-like" morphology. With a TB concentration range of 10^{-7} M to 10^{-3} M and a calculated LOD of 3.08×10^{-8} M, this sensing platform demonstrates promising applicability not only in the detection and monitoring of pesticide residues but also in broader sensing applications across various fields.

ABBREVIATIONS

Ag NPs: silver nanoparticles
CZZ: Co-Zn-ZIF
EDS: energy-dispersive X-ray spectroscopy
FCC: face-centered cubic
FP: filter paper
FE-SEM: field-emission scanning electron microscopy
LSPR: localized surface plasmon resonance
LOD: detection of limited
SERS: surface-enhanced Raman scattering
TB: tebuconazole
UV-Vis: ultraviolet-visible spectroscopy
XRD: X-ray diffraction
ZIF: zeolitic imidazolate framework

COMPETING INTERESTS

The author(s) declare that they have no competing interests.

AUTHORS' CONTRIBUTIONS

All the authors read and corrected the submitted final version.

Nguyen Bao Tran, Do Thao Anh conceived experiments design, analyzed data, carried out, and wrote the manuscript with support from Dr. Nhu Hoa Thi Tran. Nguyen Do Quynh Nhu, Le Hong Tho carried out the experiments in group. Hanh Kieu Thi Ta, Quang Ngoc Tran have supported the analysis techniques. Dr. Nhu Hoa Thi Tran revised and corrected the manuscript.

ACKNOWLEDGEMENTS

This research is funded by Vietnam National University, Ho Chi Minh City (VNU-HCM) under grant number VL2025-18-01. We would like to gratefully acknowledge the Center for Innovative Materials and Architectures (Laboratory for Optics and Sensing) at Vietnam National University in Ho Chi Minh City.

REFERENCES

1. Jutková A JZ, T K, J S. Vibrational characterization of the pesticide molecule Tebuconazole. Spectrochim Acta A Mol Biomol Spectrosc. 2022;268:120629.
2. M B, J W, A B, J K. Effects of Tebuconazole Application on SoilMicrobiota and Enzymes. Molecules. 2022;27(21).
3. B D. A comprehensive review on toxicological mechanisms and transformation products of tebuconazole: Insights on pesticide management . Science of the Total Environment Elsevier. 2024;908:168264.
4. MD H, V N, LG D, BA R, F B, de Oliveira ARM. In vitro enantioselective study of the toxicokinetic effects of chiral fungicide tebuconazole in human liver microsomes. Ecotoxicol Environ Saf. 2019;181:96–105.
5. L J, JYR S, WS S, ZU W, HL J. Metal–organic frameworks: Structures and functional applications. Materials Today Elsevier. 2019;27:43–68.

6. P K, A D, KH K. Metal organic frameworks for sensing applications. TrAC - Trends in Analytical Chemistry Elsevier. 2015;73:39–53.
7. L Y, Y Y, L X, R M, F J, X X. Large range localized surface plasmon resonance of Ag nanoparticles films dependent of surface morphology. Appl Surf Sci. 2016;367:563–568.
8. Y F, M Y, L Z, T Z, S W, L L, et al. Electrostatic self-assembly of ZIF-8/Ag nanocomposites as versatile SERS substrates for sensitive detection of environmental pollutants. Microchemical Journal. 2025;208:112612.
9. and Li W and Nguyen W and Chen W and Wang J SW, M C. Advances of metal organic frameworks in analytical applications. Materials Today Advances Elsevier. 2022;15:100273.
10. YW W, Di HX, L J, QL S, XL W. An all-in-one magnetic SERS nanosensor for ratiometric detection of Escherichia coli in foods. Anal Bioanal Chem. 2021;413(21):5419–5426.
11. NTT P, TA N, VT H, LH T, DT A, HKT T, et al. Sensors for Detection of the Synthetic Dye Rhodamine in Environmental Monitoring Based on SERS. Micromachines Multidisciplinary Digital Publishing Institute. 2022;13:1840.
12. WR P, Y C, J F, A B, LD Z. SERS Biomedical Applications: Diagnostics, Forensics, and Metabolomics. In: Frontiers and Advances in Molecular Spectroscopy Elsevier. 2017;p. 327–367.
13. T VD. Surface-enhanced Raman spectroscopy using metallic nanostructures. In: TrAC - Trends in Analytical Chemistry Elsevier. 1998;p. 557–582.
14. X C, Y L, Q F, H Q, J L, K Y, et al. An efficient modulated synthesis of zirconium metal–organic framework UiO-66 . RSC Adv [Internet] . 2022;12(10):6083–6092. Available from: https://pubs.rsc.org/en/content/articlehtml/2022/ra/d1ra07848h.
15. SA A, D B, HA K, MN H, HM A, SK P. Enhanced Water Stability and Photoresponsivity in Metal-Organic Framework (MOF): A Potential Tool to Combat Drug-resistant Bacteria. Sci Rep. 2019;9(1).
16. T S, Y L, Y Z, DQ Y, E S. Improved adhesion of Ag NPs to the polyethylene terephthalate surface via atmospheric plasma treatment and surface functionalization. Appl Surf Sci. 2017;411:8.
17. WH B, AC R, SN K, L LS, P C, AM K. Evolution of the Spin Magnetic Moments and Atomic Valence of Vanadium in VCux+, VAgx+, and VAux+ Clusters (x = 3-14). Journal of Physical Chemistry A. 2017;121(15).
18. DK P, RK R, E AK, SK S. Core-Shell Zeolitic Imidazolate Frameworks for Enhanced Hydrogen Storage. ACS Omega. 2018;3(1):167–175.
19. Bin AM, K S, M D, WMZW Y, NA I. Synthesis and characterization of silver/clay nanocomposites by chemical reduction method. Am J Appl Sci. 2009;6(11):1909–1914.
20. JM Z, Q H, J L, J Y, T P, et al. Cellulose-Derived Highly Porous Three-Dimensional Activated Carbons for Supercapacitors. ACS Omega. 2018;3(11):14933–14941.
21. L P, LM LM. Towards low-cost flexible substrates for nanoplasmonic sensing. Physical Chemistry Chemical Physics. 2013;15(15):5288–5300. Available from: https://pubs.rsc.org/en/content/articlehtml/2013/cp/c2cp43642f.
22. B H, H P, DW S. Multifunctional cellulose based substrates for SERS smart sensing: Principles, applications and emerging trends for food safety detection. Trends Food Sci Technol. 2021;110:304–320. Available from: https://www.sciencedirect.com/science/article/pii/S0924224421001060?via%3Dihub.
23. SAO W, Van Zyl E, SA O, Van Zyl ÁWE. A review of cellulose-based substrates for SERS: fundamentals, design principles, applications. Cellulose. 2019;26(11):6489–6528. Available from: https://link.springer.com/article/10.1007/s10570-019-02580-0.
24. V E, H S, E K, MH H, S M, D R, et al. Surface-Enhanced Raman scattering (SERS) filter paper substrates decorated with silver nanoparticles for the detection of molecular vibrations of Acyclovir drug. Spectrochim Acta A Mol Biomol Spectrosc. 2023;298:122762. Available from: https://www.sciencedirect.com/science/article/pii/S138614252300447X?via%3Dihub.
25. S S, V S, S M, A D. Enhanced electrochemical performance of nickel intercalated ZIF-67/rGO composite electrode for solid-state supercapacitors. Int J Hydrogen Energy . 2020;45(55):30859–30869. Available from: https://www.sciencedirect.com/science/article/pii/S0360319920330792?via%3Dihub#abs0020.
26. C S, A S, K M, S A. Zeolite Imidazolate Framework-BasedPlatform for the Electrochemical Detection of Epinephrine. J Electrochem Soc. 2023;170(10):107504. Available from: https://iopscience.iop.org/article/10.1149/1945-7111/acff21.
27. S T, K F, Y M, M M, Y H, T M, et al. Adsorption and Diffusion Phenomena in Crystal Size Engineered ZIF-8 MOF. Journal of Physical Chemistry C . 2025;119(51):28430–28439. Available from: https:/doi/pdf/10.1021/acs.jpcc.5b09520.
28. de OR, AC S. Plasmonic photocatalytic degradation of tebuconazole and 2,4-dichlorophenoxyacetic acid by Agnanoparticles-decorated TiO2 tracked by SERS analysis. . Chemosphere. 2023;338:139490.
29. and Jutková A JZ, T K, J S. Vibrational characterization of the pesticide molecule Tebuconazole. Spectrochim Acta A Mol Biomol Spectrosc. 2022;268.
30. PL T, VTC D, Van TV. Rapid Detection of Tebuconazole Basedon Aptasensor and Aggregation of Silver Nanoparticles. J Nanomater. 2021;1:5532477. Available from: http:/doi/pdf/10. 1155/2021/5532477.
31. L H, T Y, and Li F SZ, M W, X H. Generation of highly sensitive monoclonal antibody of tebuconazole: Lateral flow immunoassay application and recognition mechanism. Microchemical Journal. 2024;Available from: https://www.sciencedirect.com/science/article/pii/S0026265X24018071?via%3Dihub.
32. A S, E R, V S, K B, E MS, N S, et al. Analysis of tebuconazole residues in coconut water, kernel and leaves using LC–MS/MS. Food Chem. 2021;359:129920.
33. Šelešovská R, R S, K K, K SP, T M, O M. Electrochemical behavior of fungicide tebuconazole and its voltammetric determination on an oxygen-terminated boron-doped diamond electrode. Journal of Electroanalytical Chemistry. 2023;930:117155. Available from: https://www.sciencedirect.com/science/article/pii/S1572665723000152?via%3Dihub.
34. F M, E M, L A, C C, BB C, MJ S, et al. Novel yeast-based biosensor for environmental monitoring of tebuconazole. Appl Microbiol Biotechnol;108(1):1–12. Available from: https://link.springer.com/article/10.1007/s00253-023-12944-z.
35. M C, X L, B S, X J, J X, F F, et al. Rapid detection of tebuconazole based on hydrogel SERS chips. Talanta. 2024;277:126309.
36. J L, J C, J D, M X, M W, J W. Detection of myclobutanil and tebuconazole in apple using magnetic molecularly imprinted polymer surface-enhanced Raman spectroscopy. Journal of Food Composition and Analysis. 2024;133:106380. Available from: https://www.sciencedirect.com/science/article/pii/S0889157524004149?via%3Dihub.
37. Jutková A JZ, T K, J S. Vibrational characteriza- tion of the pesticide molecule Tebuconazole. Spectrochim Acta A Mol Biomol Spectrosc. 2022;268:120629. Available from: https://www.sciencedirect.com/science/article/pii/S1386142521012063?via%3Dihub.
38. S D, Q S, and Wu J ZZ, J F. Colorimetric and SERS dual-signal immunochromatographic assay based on AuDTNB@Ag for the detection of triadimefon. Colloids Surf A Physicochem Eng Asp;692:133978. Available from: https://www.sciencedirect.com/science/article/pii/S0927775724008392?via%3Dihub.